Geophysical Research Letters

RESEARCH LETTER
10.1029/2022GL097799

Special Section:
Using radiative-convective equilibrium to understand convective organization, clouds, and tropical climate

Westward-Propagating Moisture Mode Over the Tropical Western Hemisphere

Víctor C. Mayta[1,2], Ángel F. Adames[1], and Fiaz Ahmed[3]

[1]Department of Atmospheric and Oceanic Sciences, University of Wisconsin–Madison, Madison, WI, USA, [2]Department of Climate and Space Science and Engineering, University of Michigan, Ann Arbor, MI, USA, [3]Department of Atmospheric and Oceanic Sciences, University of California, Los Angeles, Los Angeles, CA, USA

Abstract A westward-propagating Rossby-like wave signal is found to explain a large fraction of the intraseasonal variance in cloud brightness over the Western Hemisphere. A series of diagnostic criteria suggest that this wave is a moisture mode: its moisture anomalies dominate the distribution of moist static energy (MSE) and are in phase with the precipitation anomalies; and the thermodynamic equation obeys the weak temperature gradient approximation. The wave propagates westward due to zonal moisture advection by the mean flow and is maintained by radiative heating and meridional moisture advection. These properties compare favorably with the westward propagating Rossby mode in an equatorial beta-plane model with prognostic moisture, mean meridional moisture gradient, and mean zonal wind. These results underscore the importance of water vapor in the dynamics of slowly evolving tropical systems, and the limitations of dry shallow water theory that rely on a "reduced equivalent depth" to represent moist dynamics.

Plain Language Summary Recent studies have shown that water vapor plays a crucial role in the occurrence and organization of tropical rainfall, leading to the existence of moisture modes. Such waves do not exist in the dry theory of tropical waves. While this acknowledgment has significantly advanced our understanding of tropical meteorology, most studies on how moisture and the large-scale circulation couple have been focused on the equatorial eastern hemisphere. In this study, we examine the features of a westward-propagating signal that has received relatively little attention. On the basis of several objective criteria, we show that this wave has properties consistent with moisture modes. We show evidence that this is the case by investigating the thermodynamic budget of this wave, which is shown to be consistent with the budget of a theoretical moisture mode. Our results underscore the importance of water vapor in the governing dynamics of tropical waves, and the need to move away from dry theory as a basis to understand convectively coupled tropical motions.

Key Points:

- A westward-propagating mode is found to explain a large fraction of the intraseasonal rainfall variance over the Western Hemisphere
- The processes that govern this mode are distinct from the equatorial Rossby waves from Matsuno's theory, instead being more consistent with a moisture mode
- Results underscore the need to move away from dry theory to understand slow convectively coupled tropical systems

Supporting Information:

Supporting Information may be found in the online version of this article.

Correspondence to:

V. C. Mayta,
mayta@wisc.edu

Citation:

Mayta, V. C., Adames, Á. F., & Ahmed, F. (2022). Westward-propagating moisture mode over the tropical Western Hemisphere. *Geophysical Research Letters*, *49*, e2022GL097799. https://doi.org/10.1029/2022GL097799

Received 16 JAN 2022
Accepted 27 FEB 2022

Author Contributions:

Conceptualization: Víctor C. Mayta, Ángel F. Adames
Formal analysis: Víctor C. Mayta, Fiaz Ahmed
Investigation: Ángel F. Adames, Fiaz Ahmed
Methodology: Víctor C. Mayta, Ángel F. Adames, Fiaz Ahmed
Supervision: Ángel F. Adames
Validation: Ángel F. Adames

1. Introduction

Convectively coupled atmospheric waves are often viewed as an extension of dry waves but with a reduced static stability arising from the latent heat release in convection (Haertel & Kiladis, 2004; K. A. Emanuel et al., 1994). However, in recent years it has become clear that interactions between moisture, convection, radiation and circulation are important for the dynamics of convectively coupled waves, especially at the intraseasonal (~10–100 days) time scale (Á. F. Adames & Kim, 2016; Á. F. Adames & Maloney, 2021; F. Ahmed, 2021; Gonzalez & Jiang, 2019; Raymond, 2001; A. Sobel & Maloney, 2013; A. H. Sobel et al., 2001; Wang & Sobel, 2021). These interactions can cause the dynamics of these waves to significantly differ from those described by dry shallow water theory. Furthermore, simple models of convectively coupled waves with prognostic moisture have revealed the existence of moisture modes, which do not exist in dry theory, and whose dynamics are governed by the evolution of moisture (F. Ahmed et al., 2021; Neelin & Yu, 1994; A. H. Sobel et al., 2001; Sugiyama, 2009). The primary signatures of moisture modes are strong moisture tendencies and weak temperature tendencies (Á. Adames et al., 2019; Á. F. Adames & Maloney, 2021; F. Ahmed et al., 2021). The former condition manifests as a tight coupling between moisture and precipitation. The latter ensures that the weak temperature gradient approximation (WTG; A. H. Sobel et al., 2001) is the dominant column energy balance.

An increasing number of studies show that slow, intraseasonal disturbances are better characterized as moisture modes (Á. Adames et al., 2019; Inoue et al., 2020; Raymond & Fuchs, 2009). Most of these studies (Á. F. Adames & Kim, 2016; Kang et al., 2021) have focused on the Madden-Julian Oscillation (MJO), the dominant mode of

Writing – original draft: Víctor C. Mayta, Fiaz Ahmed
Writing – review & editing: Ángel F. Adames

tropical intraseasonal variability (Jiang et al., 2020; Madden & Julian, 1994; Zhang, 2005). However, recent theoretical (F. Ahmed et al., 2021; Fuchs-Stone et al., 2019) and observational (Gonzalez & Jiang, 2019) studies suggest that equatorial Rossby waves (ER) might be moisture modes as well. Gonzalez and Jiang (2019) report the existence of slow ER modes over the Indo-Pacific Warm Pool with properties of moisture modes. This finding matches the theoretical expectation that moisture modes will preferentially occur over the Warm Pool due to the high column water vapor content observed in this region and the impact that moisture fluctuations in this region have on tropical rainfall (Á. Adames, 2017; Kang et al., 2021; Roundy & Frank, 2004). However, in this study, we find that ER modes over the tropical Western Hemisphere (TWH) are also better characterized as moisture modes. Our focus on the TWH region is motivated by the sparse literature on ER waves over this region, despite a significant contribution from ER waves to TWH rainfall variability (Figure S1a in Supporting Information S1).

In Section 2, we discuss the statistical methods used to extract the intraseasonal westward-propagating (ISWP) signal over TWH region. In Section 3, we elucidate the horizontal and vertical structures of ISWP mode. In Section 4, we examine the leading thermodynamic properties of the ISWP and show that they are consistent with moisture modes using a set of objective criteria developed by Á. Adames et al. (2019) and F. Ahmed et al. (2021). In Section 5, we examine the MSE budget of the ISWP mode and highlight the dominant processes that contribute to its maintenance and propagation. While dry shallow water theory explains the structural features of the ISWP wave, it cannot explain the primary thermodynamic properties and propagation characteristics of the ISWP mode. We address this in Section 6 using an equatorial beta-plane model with prognostic moisture, including advective interactions with the background fields. This model is similar to that of F. Ahmed (2021), and is adept at reproducing both the ISWP horizontal structure and the leading terms in the MSE budget. The results highlight the importance of prognostic water vapor fluctuations and advective interactions with the background fields in slowly evolving waves, even outside the warm pool. The results also suggest that dry shallow water theory must be supplemented with prognostic moisture variations to better describe these systems.

2. Data and Methods

2.1. Satellite CLAUS T_b and Reanalysis Data Set

Satellite-observed brightness temperature (T_b) data is used in this study as a proxy for convection. The data is obtained from the Cloud Archive User System (CLAUS) satellite data (Hodges et al., 2000). Three-dimensional (27 pressure levels) fields from the European Centre for Medium-Range Weather Forecasts ERA-5 reanalysis (ERA5; Hersbach et al., 2019) are used for analyses of the physical structures associated with the ISWP mode. The ERA5 data set utilizes a 0.5° horizontal resolution grid, with 4 times daily analyses that match the CLAUS T_b data for the 36 yr time period 1984 through 2015. We make use of the zonal, meridional and vertical winds (u, v, ω), specific humidity (q), temperature (T), diabatic heating rate (Q_1), surface and top of the atmosphere radiative fluxes, surface sensible and latent heat fluxes (SH and LE, respectively), and precipitation (P). We also use twice daily radiosonde data for Manaus (59.98°W, 3.15°S) and Belem (48.48°W, 1.48°S) obtained from the Integrated Global Radiosonde Archive – IGRA (Durre et al., 2006) for the 14 yr period from 2000 to 2013. Finally, we make use the constrained variational analysis product for the GOAmazon 2014/2015 field campaign (VARANAL; Tang et al., 2016).

2.2. Filtering of CLAUS T_b Data and EOF Analysis

To explore the ISWP mode over TWH, T_b is filtered using a fast Fourier transform retaining westward-only wavenumbers and periods between 10 and 96 days. Considering that filtered anomalies include background noise, we use Empirical Orthogonal Function (EOF) analysis to extract the dominant mode associated with ISWP mode. The EOF analysis was applied to the filtered T_b data over TWH region (5°S–20°N, 120°W-0°). The leading pair of EOFs is found to correspond to the ISWP mode, together accounting for 26% of the total variance of the westward-propagating component of T_b. Table 1 summarizes the details of the filtering and EOF analysis techniques.

2.3. Linear Regression

The PC1 time series of the T_b ISWP mode is regressed against raw T_b and ERA5 fields to obtain a composite of the wave evolution. Similarly, the relationship between the ISWP mode and MSE budget terms was determined

Table 1
Characteristics of the ISWP Mode Over Tropical Western Hemisphere

Filter	Acronym	Direction	Period (days)	k
–	ISWP	westward-only	10–96	$-\infty$ to 0
EOF	Lon domain	Lat domain	Phase speed (c_p)	Wavelength (λ)
–	120°–0°	5°S–20°N	5.4 m s^{-1}	58°

Note. (Upper row) the filter settings for the period and the wavenumber (k). (Bottom row) spatial domain for the EOF calculation. Propagation characteristics of the ISWP mode is determined by using the Radon Transform (Mayta et al., 2021). EOF, Empirical Orthogonal Function; ISWP, intraseasonal westward-propagating.

using linear regression, following the same procedure as previous studies (e.g., Á. F. Adames et al., 2021; Mapes et al., 2006; Mayta & Adames, 2021; Snide et al., 2021). Then, the perturbations are scaled to one standard deviation of the corresponding ISWP wave at zero lag. The statistical significance of these results is then assessed based on the two-tailed Student's t-test. This method takes into account the correlation coefficients and an effective number of independent sample (degrees of freedom) based on the decorrelation timescale (Livezey & Chen, 1983).

3. Large-Scale Horizontal and Vertical Structure of the ISWP Mode

Figure 1 shows the evolution of the T_b and circulation of the ISWP mode at the 850-hPa and 200-hPa levels. The convective anomalies propagate at ~5.4 m s^{-1} westward from the tropical North Atlantic (0°–25°N, 70°W–20°E) at day 0 (Figure 1a) and reach the eastern north Pacific and Central America at day +10 (Figure 1d). At 850 hPa, an anticyclone is seen propagating westward with the T_b anomalies (Figure 1a). The enhanced convection is nearly in phase with poleward flow associated with this anticyclone. At 200-hPa, the circulation features more closely resemble the structure of the $n = 1$ ER wave documented in Yang et al. (2007) and Kiladis et al. (2009),

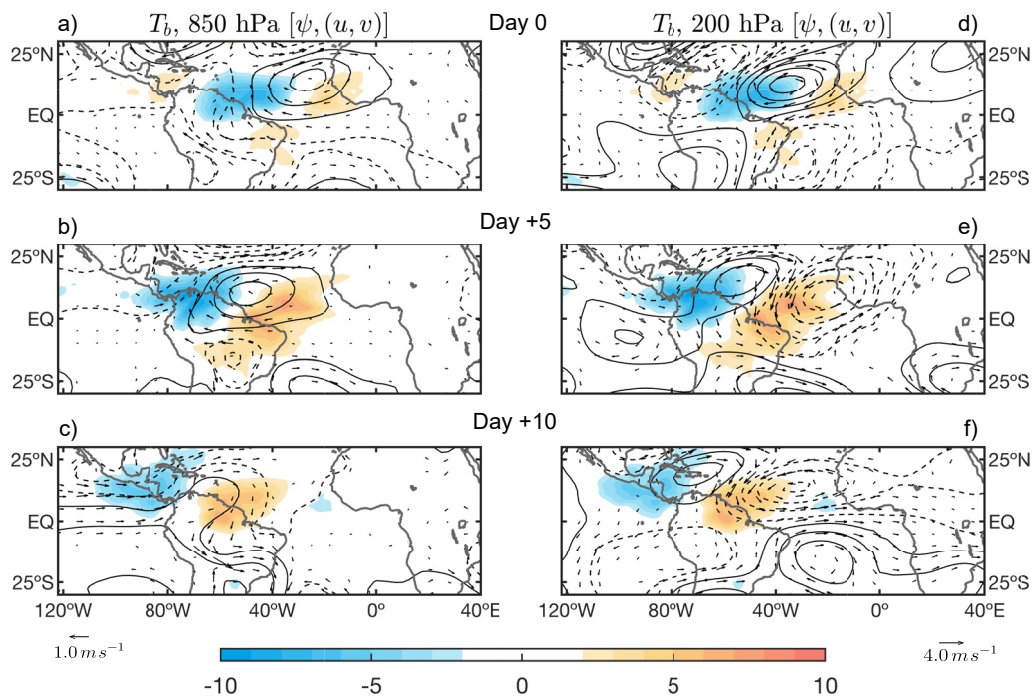

Figure 1. Anomalous T_b (shading, in units of K), streamfunction (contours), and wind (vectors) regressed onto PC1 of the ISWP mode at 850 hPa (left panels) and 200 hPa (right panels) for the 1998–2015 period and all 12 calendar months. Time lags go from day 0 to day +10, with day 0 representing maximum convection around 60°W. Streamfunction contour interval is 2.0×10^6 m^2 s^{-1}, with negative contours dashed. The shaded and contoured regions are statistically significant at the 95% level. Wind vectors are plotted only where either the u or v component is significant at the 95% level or greater.

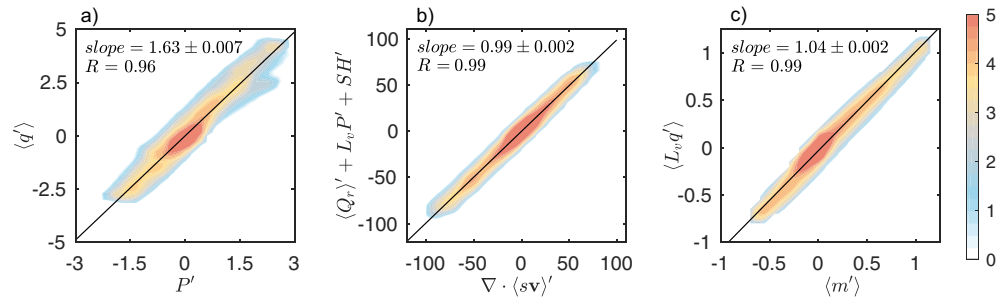

Figure 2. Scatterplots of (a) P′ versus $\langle q' \rangle$, (b) $\nabla \cdot \langle s\mathbf{v} \rangle'$ versus $\langle Q_r \rangle' + L_v P' + SH'$, and (c) $\langle m' \rangle$ versus $\langle L_v q' \rangle$. The shading represents the base-10 logarithm of the number of points within 0.2×0.2 mm bins in (a), 5 W m^{-2} × 5 W m^{-2} bins in (b), and 5×10^{-4} J m^{-2} × 5×10^{-4} J m^{-2} bins in (c). Anomalies are obtained by regressing all fields against the PC1 (normalized, ISWP) over the TWH region (120°W–0°, 5°S–10°N). The linear fit obtained from linear least squares fit is shown as a solid black line. The slope of the linear fit and the correlation coefficient are shown in the top-left of each panel.

with pairs of cyclonic and anticyclonic gyres straddling near-equatorial convection (Figure 1d). When the upper and lower troposphere are considered together, we see that the ISWP mode structure starts off barotropic (e.g., Figures 1a and 1d), and slowly becomes more baroclinic as it propagates westward (day +5 onward). The out of phase relationship between the lower and upper troposphere also resembles the structure documented in Yang et al. (2007) for the Western Hemisphere ER waves.

Even though the convection associated with the ISWP mode is mostly off-equatorial, its circulations features resemble the theoretical shallow water structure of an equatorially trapped ER wave (Kiladis et al., 2009; Matsuno, 1966; Wheeler et al., 2000). However, its slow westward propagation of 5.4 m s^{-1} is difficult to explain with dry shallow water theory alone. It would require a reduction of the equivalent depth from ∼250 m, the depth that yields the observed phase speed of dry gravity waves to a mere 5 m. Thus, other physical processes must occur in the ISWP mode that make it distinct from dry shallow water ER waves.

4. Evidence That the ISWP Wave Is a Moisture Mode

The slow propagation of the ISWP mode suggests that it may have properties of a moisture mode. To test this possibility, we will examine the three criteria described by F. Ahmed et al. (2021) that moisture modes must satisfy, modifying them to make them more suitable to for their diagnosis in observational, model and reanalysis data. We will also examine the criteria outlined by Á. Adames et al. (2019). These criteria are:

1. Moisture anomalies must exhibit a high coherence with precipitation anomalies.

For a disturbance to be considered a moisture mode, its signature in column water vapor ($\langle q \rangle$, where $\langle \cdot \rangle \equiv 1/g \int_{100}^{1000} (\cdot) dp$) must be sufficiently large to significantly modulate surface precipitation (P'). This should result in a strong correlation between P' and $\langle q' \rangle$. We apply this criteria to the ISWP by constructing a scatterplot between P' and $\langle q' \rangle$. A strong linear correlation of 0.96 is observed (Figure 2a), and anomalies in $\langle q' \rangle$ of 2.5 mm are associated with anomalies in P' of 1.5 mm/day, which satisfy this first criterion.

2. The mode must obey the weak temperature gradient (WTG) balance at the leading order in its temperature budget.

Following Inoue and Back (2015), the WTG approximation in the column-integrated dry static energy (DSE) budget can be expressed as:

$$\nabla \cdot \langle s\mathbf{v} \rangle \simeq \langle Q_1 \rangle \tag{1}$$

where $s = C_p T + \Phi$ is DSE, $\mathbf{v} = u\mathbf{i} + v\mathbf{j}$ is the horizontal vector wind field, and Q_1 is the apparent heating rate, which can be calculated from ERA5 reanalysis data following Yanai and Johnson (1993):

$$\langle Q_1 \rangle \simeq \langle Q_r \rangle + L_v P + SH \tag{2}$$

where Q_r is the radiative heating rate, SH is the surface sensible heat flux, and L_v represents the latent heat of vaporization (2.5×10^6 J kg $^{-1}$).

The individual terms in the balance implied by Equation 1 must be at least an order of magnitude larger than the temperature tendency over region of maximum convection. From the scatterplot of Figure 2b we see a robust relationship between them, with a high correlation coefficient of 0.99 and slope of ≈1. Therefore, the ISWP mode is in WTG balance at the leading order.

3. Thermodynamic variations in the mode must be dominated by moisture

Moisture modes occur when moisture is the main contributor to moist static energy (MSE, m). From Figure 2c, we can see that $L_v q'$ explains nearly all of the m' variance, and exhibits a near one to one relationship with m'. Thus, we can make the following approximation for the ISWP mode $m' = C_p T' + \Phi' + L_v q' \approx L_v q'$.

4. N_{mode} parameter

N_{mode} is a nondimensional parameter that measures the relative contribution of moisture and temperature to the evolution of moist enthalpy. When $N_{mode} \ll 1$, moisture governs the thermodynamics of a wave, resulting in moisture modes. Thus, N_{mode} can be thought of as an independent measure of criterion (c). This parameter can be easily estimated as $N_{mode} \approx \left|\frac{C_p T'}{L_v q'}\right|$, giving a value of N_{mode} of ∼0.1 from ERA5 and soundings (Figure S3 in Supporting Information S1). A more strict definition of N_{mode} can be computed as in Á. Adames et al. (2019):

$$N_{mode} \equiv \frac{c_p^2 \tau}{c^2 \tau_c} \tag{3}$$

where c is the phase speed of a first baroclinic free gravity wave ($c \simeq 50\ ms^{-1}$), and $\tau_c = \langle q' \rangle / P'$ is the convective moisture adjustment time scale. For the ISWP mode the calculated phase speed (c_p) is 5.4 ms^{-1} so that $c_p/c \sim 0.108$. From Table 1 we can estimate τ to be roughly 13.7 days, where $\tau = \lambda / c_p = 58 \times 111.319\ km \times \cos(\varphi) / (5.4\ ms^{-1})$, and $111.319\ km \times \cos(\varphi)$ is the length of a degree longitude at latitude $\varphi = 5°$ N. $\tau_c = 1.6$ days can be estimated from Figure 2a, yielding $\tau/\tau_c \approx 8.6$. Combining the two results we obtain $N_{mode} \approx 0.10$. Thus, the ISWP mode can be categorized as a moisture mode according to the N_{mode} criterion.

In the Supporting Information, we also show one last criterion based on the effective Gross Moist Stability (Γ_{eff}), which the ISWP mode also satisfies. Thus, the ISWP mode satisfies all the criteria necessary to be considered a moisture mode.

5. Moist Static Energy Budget

That $L_v q$ governs the distribution of MSE and is highly correlated with rainfall implies that we can use the MSE budget to understand the evolution of convection in the ISWP mode. The column-integrated MSE budget is written as:

$$\frac{\partial \langle m \rangle}{\partial t} = -\langle \mathbf{v} \cdot \nabla m \rangle - \left\langle \omega \frac{\partial m}{\partial p} \right\rangle + \langle Q_r \rangle + LE + SH \tag{4}$$

where the first and second terms on the right-hand side of Equation 4 are the horizontal and vertical MSE advection, respectively. The remaining terms on Equation 4 are the MSE source terms: Q_r, the surface latent heat flux (LE), and SH.

Figure 3 shows the anomalous MSE budget terms from Equation 4 in the same format as Figure S1b in Supporting Information S1. It is clear from comparing the six panels that horizontal advection is the largest contributor to the MSE tendency, exhibiting a similar magnitude and a near in-phase relation with it. Column-integrated radiative heating, on the other hand, is the second-largest term and is approximately in phase with the MSE itself but in quadrature with the MSE tendency (Figure 3d). The column-integrated vertical MSE advection (Figure 3c) and $\langle Q_r \rangle$ are of similar amplitude and roughly cancel one another. Finally, surface fluxes (Figure 3e) vary almost in phase with vertical MSE advection and out of phase with $\langle Q_r \rangle$. A residual exists in the budget that is of a comparable magnitude to the vertical MSE advection (Figure 3d). This residual has been documented in the ERA5 data

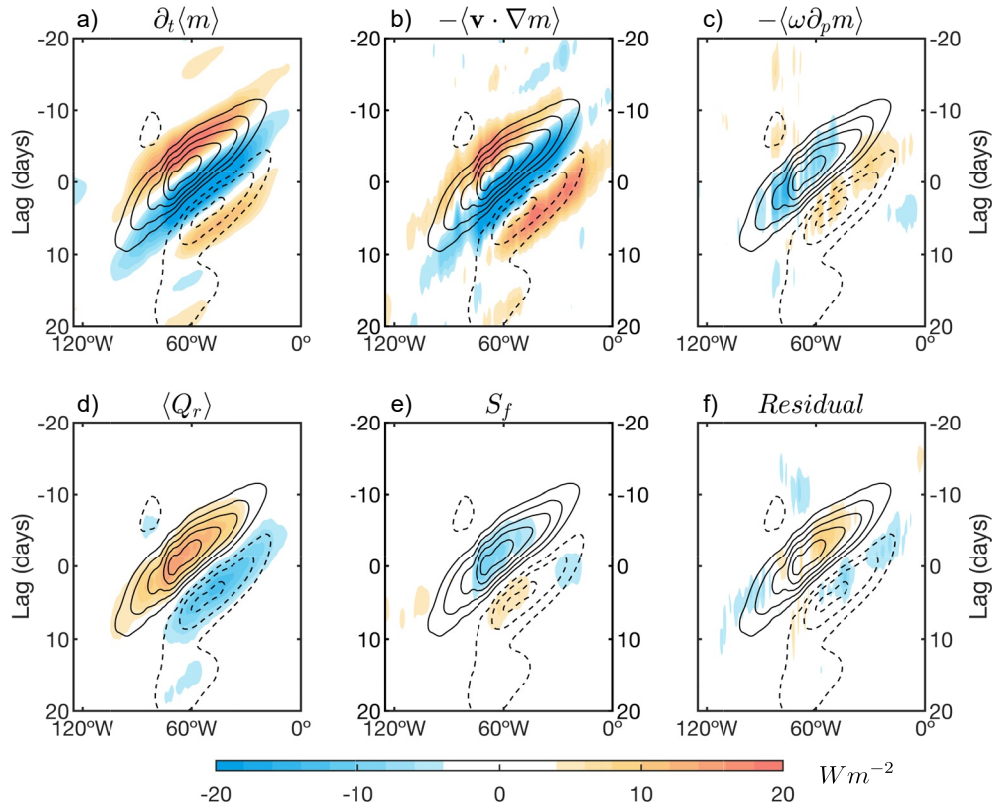

Figure 3. Time-longitude diagram of 5°S – 10°N column-integrated MSE (contour) and MSE budget terms (shading) regressed onto PC1 (normalized, ISWP) (top) Advective MSE terms: (a) $\partial_t\langle m\rangle$, (b) $-\langle \mathbf{v}\cdot\nabla m\rangle$, (c) $-\langle\omega\partial_p m\rangle$ (bottom) Source MSE terms: (d) $\langle Q_r\rangle$, (e) surface fluxes ($S_f = LE + SH$), and (f) residual. The contour interval for $\langle m\rangle$ is 2×10^6 J m^{-2}.

(Ren et al., 2021), and is hypothesized to be due to an improper representation of convection in the reanalysis, in a similar vein to what Mapes and Bacmeister (2012) documented for MERRA-2 data.

Following previous studies (e.g., Á. Adames, 2017; Andersen & Kuang, 2012), we can more objectively quantify the contribution of different processes to the propagation and maintenance of the ISWP mode by projecting them upon the MSE tendency and the MSE anomalies. The regression corresponding to each budget term is multiplied by the regression of the $\partial_t\langle m\rangle$ and $\langle m\rangle$ and then divided by the area-weighted square of themselves.

The results of this projection, shown in Figure 4, reveal that horizontal MSE advection is the largest contributor to the westward propagation of the ISWP (Figure 4a). To understand in more detail how horizontal MSE advection governs the propagation of the MSE anomalies, we decompose it into the following contributions (Figure 4 and S5 in Supporting Information S1):

$$-\langle u\partial_x m\rangle \approx -\langle\bar{u}\partial_x m'\rangle - \langle u'\partial_x\bar{m}\rangle - \langle u'\partial_x m'\rangle \tag{5a}$$

$$-\langle v\partial_y m\rangle \approx -\langle\bar{v}\partial_y m'\rangle - \langle v'\partial_y\bar{m}\rangle - \langle v'\partial_y m'\rangle \tag{5b}$$

where the overbar represents the low-frequency component, obtained from a 96 days lowpass filter, and the primes are departures from this low-frequency component.

The leading term associated with westward propagation is the horizontal advection of the MSE anomalies by the low-frequency zonal wind ($\langle\bar{u}\partial_x m'\rangle$). Propagation of ER waves over western Pacific is also governed by the same process (Gonzalez & Jiang, 2019). All other contributions are much smaller and will not be discussed.

Figure 4b shows the contribution of each budget term to the maintenance of the MSE for the ISWP mode. As expected from recent studies on slowly propagating disturbances (Á. Adames, 2017; Andersen & Kuang, 2012; Benedict et al., 2020; A. Sobel et al., 2014), the column-integrated radiative heating is the largest contributor to

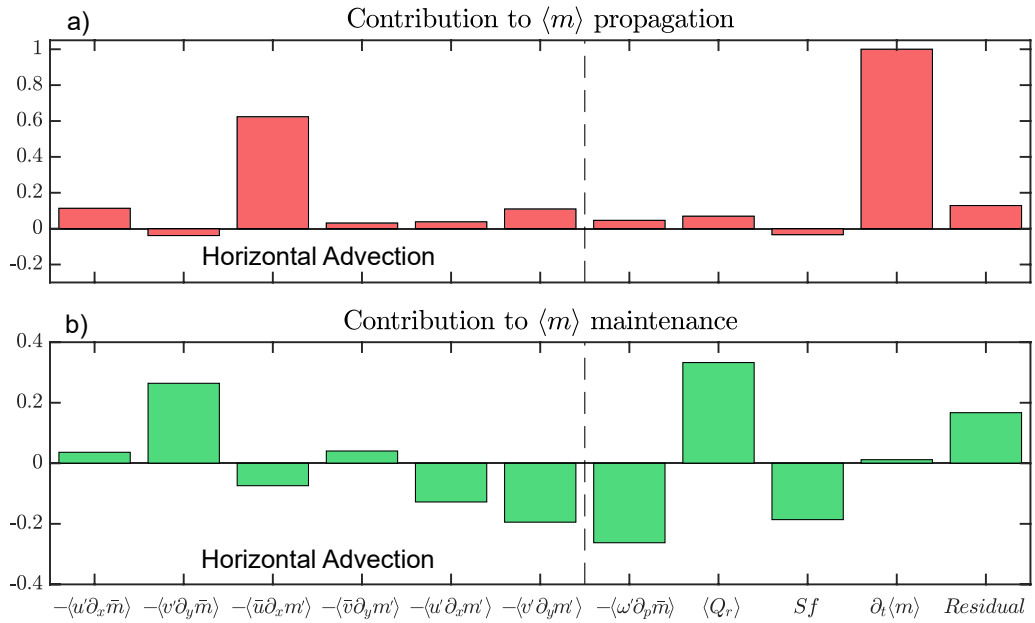

Figure 4. Normalized contribution of each term in the MSE budget Equation 4 to the (top) propagation and (bottom) maintenance of the ISWP. The contribution of each horizontal MSE advection terms are plotted in the left part of the panels.

the maintenance of the ISWP mode. The second-largest contribution to maintenance is the horizontal advection of the low-frequency MSE by the intraseasonal meridional wind ($-\langle v'\partial_y \bar{m}\rangle$). Horizontal MSE advection by high-frequency eddies, vertical MSE advection and anomalous surface fluxes act to damp the MSE anomalies.

6. Intraseasonal Westward Propagating Wave in an Equatorial Beta-Plane Model

Up to this point, we have shown that the ISWP mode has the properties of a moisture mode. Since moisture modes exhibit a behavior that are distinct from Matsuno's dry shallow water wave solutions, it is instructive to instead compare the ISWP mode to a model that accounts for the important role water vapor plays in tropical motions. In this section, we compare the horizontal structure and MSE budgets associated with ISWP mode with an equatorial beta-plane model that is similar to the model of F. Ahmed (2021). Our comparison is qualitative, and is primarily used to highlight the importance of slow moisture variations for ISWP dynamics.

The prognostic moisture equation in this model is given by:

$$\frac{\partial\langle q'\rangle}{\partial t} + \left\langle u'\frac{\partial \bar{q}}{\partial x}\right\rangle + \left\langle v'\frac{\partial \bar{q}}{\partial y}\right\rangle + \left\langle \omega\frac{\partial \bar{q}}{\partial p}\right\rangle + \left\langle \bar{U}\frac{\partial q'}{\partial x}\right\rangle = E' - \langle Q_c'\rangle. \tag{6}$$

In the above equation, q', u' and v' are the perturbation moisture and horizontal winds respectively; E' and Q_c' are the perturbation surface evaporation and convective heating respectively. The background moisture and zonal wind fields are $\bar{q}$ and $\bar{U}$ respectively. The only structural difference from the model of F. Ahmed (2021) is the inclusion of the $\langle \bar{U}\frac{\partial q'}{\partial x}\rangle$ term in Equation 6, whose importance was only apparent after the MSE budget analysis in Section 5. The value of $\bar{U}$ is set to -5 m s^{-1} to represent the background low-level easterly flow seen over TWH region (Figure S6 in Supporting Information S1). Other model details are provided in the Supporting Information S1 Section 2.

In F. Ahmed (2021) it was shown that the moist beta-plane system contains eastward and westward propagating Rossby wave solutions, and that the former closely resembles the MJO. The similarities between the westward propagating Rossby wave solution and the ISWP are now discussed. Figure 5a shows the horizontal structure of the westward propagating, $n = 1$ Rossby mode. This mode has a zonal wavenumber 5 ($k = -5$), chosen to match the peak wavenumber in the regional space-time spectrum of CLAUS T_b (Figure S1a in Supporting Information S1). Similar to observations, the theoretical mode displays two off-equatorial gyres. Convection is nearly in

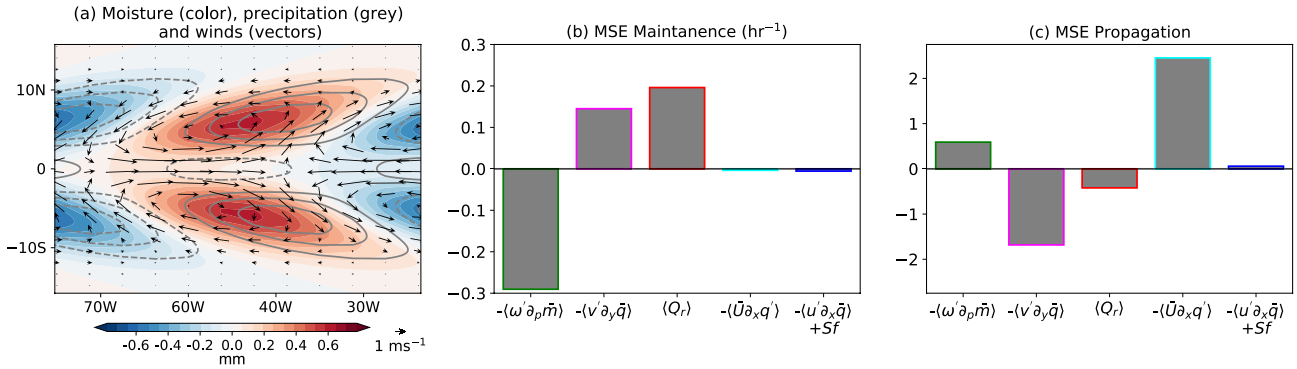

Figure 5. (a) Moisture (color), precipitation (contours), and low-level winds (vectors) for the westward-propagating zonal wavenumber-5 ($k = -5$) Rossby moisture mode discussed in Section 6. Panels (b) and (c) show the relative contribution of each MSE budget term to the (b) maintenance and (c) propagation of the MSE anomalies associated with this wave.

quadrature with the gyres—similar to Figures 1a and 1d—and nearly in phase with column moisture—as implied by the moisture mode analysis in Section 4a. The MSE budget for the theoretical mode is computed as shown in Supporting Information S1. A projection in the MSE maintenance and propagation budget terms are shown in Figures 5b and 5c respectively. The dominant processes that propagate and maintain the theoretical mode are in qualitative agreement with the observed ISWP mode (see Figure 4). Large opposing contributions to MSE maintenance by radiative heating and vertical MSE advection (Figure 4a) are reproduced in the theoretical mode. The contributions from mean meridional moisture advection to MSE maintenance is also reproduced. As in the reanalysis data, the main process responsible for the westward propagation is moisture advection by the mean zonal winds $\langle \bar{U}\partial_x q' \rangle$.

Discrepancies do exist between theory and observations. For instance, meridional moisture advection opposes the westward propagation due to the off-equatorial gyres moistening to the east of convection (F. Ahmed, 2021). This effect is smaller in the reanalysis (Figure 4b), plausibly due to asymmetries in the local meridional moisture gradient. There is a stronger negative contribution from vertical MSE advection (Figure 5b) compared to the reanalysis (Figure 4b). This effect is possibly due to the absence of stratiform heating (Schumacher et al., 2004) in the beta-plane modes; stratiform heating can oppose the MSE export by deep baroclinic heating (Raymond et al., 2009), and potentially limit the impacts of vertical MSE advection. Despite these discrepancies, there is overall qualitative agreement between theory and observed ISWP, with respect to the horizontal structures and the MSE budget.

7. Summary and Conclusions

This study showed that an intraseasonal westward-propagating (ISWP) wave over the Western Hemisphere explains a large fraction of the intraseasonal T_b variance. While the structural features of this mode are akin to the ER waves found in Matsuno's dry shallow water theory, its propagation is too slow to be easily explained by it. On the basis of four criteria based on previous work by Á. Adames et al. (2019) and F. Ahmed et al. (2021), we conclude that the ISWP is instead a moisture mode. In its MSE budget horizontal MSE advection by the mean flow governs the propagation of the MSE anomalies, which in turn are maintained by radiative heating and meridional moisture advection. The governing MSE maintenance and propagation processes are in qualitative agreement with the model of F. Ahmed (2021), in which the inclusion of prognostic moisture and a mean meridional moisture gradient causes ER waves to exhibit moisture mode behavior.

Previous theoretical and observational studies (F. Ahmed, 2021; Fuchs-Stone et al., 2019; Gonzalez & Jiang, 2019) have already shown evidence that ER waves over the Indo-Pacific warm pool are moisture modes. However, this is the first study to show evidence for the existence of moisture modes over the tropical Western Hemisphere. It is also the first study to diagnose whether a wave is a moisture mode on the basis of a series of objective criteria that are based on theory. The fact that we have identified a moisture mode in a region that is previously not known to support them suggests that these types of systems may be common. These modes are characterized by slow propagation driven by moisture fluctuations that are coupled to convection and circulation. Other tropical wave

properties such as meridional tilts and equatorial asymmetry also likely emerge from similar moist dynamics (F. Ahmed et al., 2021; K. Emanuel, 2020; Fuchs & Raymond, 2017; Wang & Sobel, 2021). These recent results highlight the limitations of shallow water equatorial wave theory without prognostic moisture variations. Moisture mode theory (Á. F. Adames & Maloney, 2021; Jiang et al., 2020; A. H. Sobel et al., 2001) may be a more reasonable starting point to understand the dynamics of these waves.

Data Availability Statement

The data set used in this study are available at ECWF (ERA5; https://doi.org/10.24381/cds.adbb2d47), the Atmospheric Radiation Measurement (ARM) program archive (VARANAL; https://iop.archive.arm.gov/arm-iop/0eval-data/xie/scm-forcing/iop_at_mao/GOAMAZON/2014-2015/) [registration is required to access data], Integrated Global Radiosonde Archive (IGRA; https://www.ncei.noaa.gov/pub/data/igra/), and the interpolated CLAUS T_b data is available at https://catalogue.ceda.ac.uk/uuid/ce476101711ce73107c9e90265ec6d9a.

Acknowledgments
VM and ÁFA were supported by the National Science Foundation under Grant AGS-1841559. FA acknowledges support from National Science Foundation grant AGS-7691936810.

References

Adames, Á. (2017). Precipitation budget of the Madden–Julian oscillation. *Journal of the Atmospheric Sciences*, *74*(6), 1799–1817. https://doi.org/10.1175/JAS-D-16-0242.1

Adames, Á., Kim, D., Clark, S. K., Ming, Y., & Inoue, K. (2019). Scale Analysis of moist thermodynamics in a simple model and the relationship between moisture modes and gravity waves. *Journal of the Atmospheric Sciences*, *76*(12), 3863–3881. https://doi.org/10.1175/JAS-D-19-0121.1

Adames, Á. F., & Kim, D. (2016). The MJO as a dispersive, convectively coupled moisture wave: Theory and observations. *Journal of the Atmospheric Sciences*, *73*(3), 913–941. https://doi.org/10.1175/JAS-D-15-0170.1

Adames, Á. F., & Maloney, E. D. (2021). Moisture mode theory's contribution to advances in our understanding of the Madden-Julian oscillation and other tropical disturbances. *Current Climate Change Reports*, *7*, 72–85. https://doi.org/10.1007/s40641-021-00172-4

Adames, Á. F., Powell, S. W., Ahmed, F., Mayta, V. C., & Neelin, J. D. (2021). Tropical precipitation evolution in a Buoyancy-budget framework. *Journal of the Atmospheric Sciences*, *78*(2), 509–528. https://doi.org/10.1175/JAS-D-20-0074.1

Ahmed, F. (2021). The MJO on the equatorial beta plane: An eastward-propagating Rossby wave induced by meridional moisture advection. *Journal of the Atmospheric Sciences*, *78*(10), 3115–3135. https://doi.org/10.1175/JAS-D-21-0071.1

Ahmed, F., Neelin, J. D., & Adames, Á. F. (2021). Quasi-equilibrium and weak temperature gradient balances in an equatorial beta-plane model. *Journal of the Atmospheric Sciences*, *78*(1), 209–227. https://doi.org/10.1175/JAS-D-20-0184.1

Andersen, J. A., & Kuang, Z. (2012). Moist static energy budget of MJO-like disturbances in the atmosphere of a zonally symmetric aquaplanet. *Journal of Climate*, *25*(8), 2782–2804. https://doi.org/10.1175/JCLI-D-11-00168.1

Benedict, J. J., Medeiros, B., Clement, A. C., & Olson, J. G. (2020). Investigating the role of cloud-radiation interactions in subseasonal tropical disturbances. *Geophysical Research Letters*, *47*(9), 1–11. https://doi.org/10.1029/2019GL086817

Durre, I., Vose, R. S., & Wuertz, D. B. (2006). Overview of the integrated global radiosonde archive. *Journal of Climate*, *19*(1), 53–68. https://doi.org/10.1175/jcli3594.1

Emanuel, K. (2020). Slow modes of the equatorial waveguide. *Journal of the Atmospheric Sciences*, *77*(5), 1575–1582. https://doi.org/10.1175/jas-d-19-0281.1

Emanuel, K. A., David Neelin, J., & Bretherton, C. S. (1994). On large-scale circulations in convecting atmospheres. *Quarterly Journal of the Royal Meteorological Society*, *120*(519), 1111–1143. https://doi.org/10.1002/qj.49712051902

Fuchs, Z., & Raymond, D. J. (2017). A simple model of intraseasonal oscillations. *Journal of Advances in Modeling Earth Systems*, *9*(2), 1195–1211. https://doi.org/10.1002/2017MS000963

Fuchs-Stone, Ž., Raymond, D. J., & Sentić, S. (2019). A simple model of convectively coupled equatorial rossby waves. *Journal of Advances in Modeling Earth Systems*, *11*(1), 173–184.

Gonzalez, A. O., & Jiang, X. (2019). Distinct propagation characteristics of intraseasonal variability over the tropical west pacific. *Journal of Geophysical Research: Atmospheres*, *124*(10), 5332–5351. https://doi.org/10.1029/2018JD029884

Haertel, P. T., & Kiladis, G. N. (2004). Dynamics of 2-day equatorial waves. *Journal of the Atmospheric Sciences*, *61*(22), 2707–2721. https://doi.org/10.1175/JAS3352.1

Hersbach, H., Bell, W., Berrisford, P., Horányi, A., M.-S, J., Nicolas, J., & Dee, D. (2019). *Global reanalysis: Goodbye era-interim, hello era5* (Vol. 04, pp. 17–24). Retrieved from https://www.ecmwf.int/node/19027doi10.21957/vf291hehd7

Hodges, K. I., Chappell, D. W., Robinson, G. J., & Yang, G. (2000). An improved algorithm for generating global window brightness temperatures from multiple satellite infrared imagery. *Journal of Atmospheric and Oceanic Technology*, *17*(10), 1296–1312. https://doi.org/10.1175/1520-0426(2000)017<1296:aiafgg>2.0.co;2

Inoue, K., Adames, Á. F., & Yasunaga, K. (2020). Vertical velocity profiles in convectively coupled equatorial waves and MJO: New diagnoses of vertical velocity profiles in the wavenumber-frequency domain. *Journal of the Atmospheric Sciences*, *77*(6), 2139–2162. https://doi.org/10.1175/JAS-D-19-0209.1

Inoue, K., & Back, L. E. (2015). Gross moist stability assessment during TOGA COARE: Various interpretations of gross moist stability. *Journal of the Atmospheric Sciences*, *72*(11), 4148–4166. https://doi.org/10.1175/JAS-D-15-0092.1

Jiang, X., Adames, n. F., Kim, D., Maloney, E. D., Lin, H., Kim, H., et al. (2020). Fifty years of research on the Madden-Julian oscillation: Recent progress, challenges, and perspectives. *Journal of Geophysical Research: Atmospheres*, *125*(17), e2019JD030911. https://doi.org/10.1029/2019JD030911

Kang, D., Kim, D., Ahn, M.-S., & An, S.-I. (2021). The role of the background meridional moisture gradient on the propagation of the MJO over the maritime continent. *Journal of Climate*, *34*(16), 6565–6581. https://doi.org/10.1175/JCLI-D-20-0085.1

Kiladis, G. N., Wheeler, M. C., Haertel, P. T., Straub, K. H., & Roundy, P. E. (2009). Convectively coupled equatorial waves. *Review of Geophysics*, *47*(2). https://doi.org/10.1029/2008rg000266

Livezey, R. E., & Chen, W. Y. (1983). Statistical field significance and its determination by Monte Carlo techniques. *Monthly Weather Review*, *111*, 46–59. https://doi.org/10.1175/1520-0493(1983)111<0046:sfsaid>2.0.co;2
Madden, R. A., & Julian, P. R. (1994). Observations of the 40–50-day tropical oscillation. *Monthly Weather Review*, *112*, 814–837. https://doi.org/10.1175/1520-0493(1994)122<0814:ootdto>2.0.co;2
Mapes, B., & Bacmeister, J. T. (2012). Diagnosis of tropical biases and the MJO from patterns in the MERRA analysis tendency fields. *Journal of Climate*, *25*(18), 6202–6214. https://doi.org/10.1175/jcli-d-11-00424.1
Mapes, B., Tulich, S., Lin, J., & Zuidema, P. (2006). The mesoscale convection life cycle: Building block or prototype for large-scale tropical waves? *Dynamics of Atmospheres and Oceans*, *42*(1), 3–29. https://doi.org/10.1016/j.dynatmoce.2006.03.003
Matsuno, T. (1966). Quasi-geostrophic motions in the equatorial area. *Journal of the Meteorological Society of Japan*, *44*, 25–43. https://doi.org/10.2151/jmsj1965.44.1_25
Mayta, V. C., & Adames, A. F. (2021). Two-day westward-propagating inertio-gravity waves during GoAmazon. *Journal of the Atmospheric Sciences*, *78*(11), 3727–3743. https://doi.org/10.1175/JAS-D-20-0358.1
Mayta, V. C., Kiladis, G. N., Dias, J., Dias, P. L. S., & Gehne, M. (2021). Convectively coupled kelvin waves over tropical South America. *Journal of Climate*, *34*(16), 6531–6547. https://doi.org/10.1175/JCLI-D-20-0662.1
Neelin, J. D., & Yu, J.-Y. (1994). Modes of tropical variability under convective adjustment and the Madden-Julian oscillation. Part I: Analytical results. *Journal of the Atmospheric Sciences*, *51*(13), 1876–1894. https://doi.org/10.1175/1520-0469(1994)051<1876:motvuc>2.0.co;2
Raymond, D. J. (2001). A new model of the Madden–Julian oscillation. *Journal of the Atmospheric Sciences*, *58*(18), 2807–2819. https://doi.org/10.1175/1520-0469(2001)058<2807:anmotm>2.0.co;2
Raymond, D. J., & Fuchs, Z. (2009). Moisture modes and the Madden–Julian oscillation. *Journal of Climate*, *22*(11), 3031–3046. https://doi.org/10.1175/2008JCLI2739.1
Raymond, D. J., Sessions, S. L., Sobel, A. H., & Fuchs, Ž. (2009). The mechanics of gross moist stability. *Journal of Advances in Modeling Earth Systems*, *1*(3). https://doi.org/10.3894/james.2009.1.9
Ren, P., Kim, D., Ahn, M.-S., Kang, D., & Ren, H.-L. (2021). Intercomparison of MJO column moist static energy and water vapor budget among six modern reanalysis products. *Journal of Climate*, *34*(8), 2977–3001. https://doi.org/10.1175/JCLI-D-20-0653.1
Roundy, P. E., & Frank, W. M. (2004). A climatology of waves in the equatorial region. *Journal of the Atmospheric Sciences*, *61*, 2105–2132. https://doi.org/10.1175/1520-0469(2004)061<2105:acowit>2.0.co;2
Schumacher, C., Houze, R. A., Jr, & Kraucunas, I. (2004). The tropical dynamical response to latent heating estimates derived from the TRMM precipitation radar. *Journal of the Atmospheric Sciences*, *61*(12), 1341–1358. https://doi.org/10.1175/1520-0469(2004)061<1341:ttdrtl>2.0.co;2
Snide, C. E., Adames, A. F., Powell, S. W., & Mayta, V. C. (2021). The role of large-scale moistening by adiabatic lifting in the Madden-Julian Oscillation convective onset. *Journal of Climate*, 269–284. https://doi.org/10.1175/JCLI-D-21-0322.1
Sobel, A., & Maloney, E. (2013). Moisture modes and the eastward propagation of the MJO. *Journal of the Atmospheric Sciences*, *70*(1), 187–192. https://doi.org/10.1175/JAS-D-12-0189.1
Sobel, A., Wang, S., & Kim, D. (2014). Moist static energy budget of the MJO during DYNAMO. *Journal of the Atmospheric Sciences*, *71*(11), 4276–4291. https://doi.org/10.1175/JAS-D-14-0052.1
Sobel, A. H., Nilsson, J., & Polvani, L. M. (2001). The weak temperature gradient approximation and balanced tropical moisture waves. *Journal of the Atmospheric Sciences*, *58*(23), 3650–3665. https://doi.org/10.1175/1520-0469(2001)058<3650:twtgaa>2.0.co;2
Sugiyama, M. (2009). The moisture mode in the quasi-equilibrium tropical circulation model. Part I: Analysis based on the weak temperature gradient approximation. *Journal of the Atmospheric Sciences*, *66*, 1507–1523. https://doi.org/10.1175/2008jas2690.1
Tang, S., Xie, S., Zhang, Y., Zhang, M., Schumacher, C., Upton, H., et al. (2016). Large-scale vertical velocity, diabatic heating and drying profiles associated with seasonal and diurnal variations of convective systems observed in the GoAmazon2014/5 experiment. *Atmospheric Chemistry and Physics*, *16*(22), 14249–14264. https://doi.org/10.5194/acp-16-14249-2016
Wang, S., & Sobel, A. H. (2021). A unified moisture mode theory for the madden julian oscillation and the boreal summer intraseasonal oscillation. *Journal of Climate*, 1–71.
Wheeler, M., Kiladis, G. N., & Webster, P. J. (2000). Large-scale dynamical fields associated with convectively coupled equatorial waves. *Journal of the Atmospheric Sciences*, *57*(5), 613–640. https://doi.org/10.1175/1520-0469(2000)057<0613:lsdfaw>2.0.co;2
Yanai, M., & Johnson, R. (1993). Impacts of cumulus convection on thermodynamic fields. In K. A. Emanuel & D. J. Raymond (Eds.), *The representation of cumulus convection in numerical models* (pp. 39–62). Meteorological Monographs. https://doi.org/10.1007/978-1-935704-13-3_4
Yang, G.-Y., Hoskins, B., & Slingo, J. (2007). Convectively coupled equatorial waves. Part I: Horizontal and vertical structures. *Journal of the Atmospheric Sciences*, *64*, 3406–3423. https://doi.org/10.1175/jas4017.1
Zhang, C. (2005). Madden-Julian oscillation. *Reviews of Geophysics*, *43*, 1–36. https://doi.org/10.1029/2004rg000158

References From the Supporting Information

Ahmed, F., Adames, A. F., & Neelin, J. D. (2020). Deep Convective Adjustment of ´ 86 87 Temperature and Moisture. *Journal of the Atmospheric Sciences*, *77*(6), 2163–2186. https://doi.org/10.1175/JAS-D-19-0227.1
Ahmed, F., & Neelin, J. D. (2018). Reverse Engineering the Tropical Precipita90 tion–Buoyancy Relationship. *Journal of the Atmospheric Sciences*, *75*(5), 1587–1608. https://doi.org/10.1175/91JAS-D-17-0333.1
Dias, J., & Kiladis, G. N. (2014). Influence of the basic state zonal flow on con93 vectively coupled equatorial waves. *Geophysical Research Letters*, *41*(19), 6904–6913. https://doi.org/10.1002/952014GL061476
Neelin, J. D., Peters, O., & Hales, K. (2009). The transition to strong convection. *Journal of the Atmospheric Sciences*, *66*(8), 2367–2384.
Neelin, J. D., & Zeng, N. (2000). A Quasi-Equilibrium Tropical Circulation Model; 109 Formulation. *Journal of the Atmospheric Sciences*, *57*, 1741–1766.
Peters, M. E., & Bretherton, C. S. (2005). A simplified model of the Walker circulation with an interactive ocean mixed layer and cloud-radiative feedbacks. *J. Climate*, *18*(20), 4216–4234.
Su, H., & Neelin, J. D. (2002). Teleconnection mechanisms for tropical Pacific descent anomalies during El Ni¢no. *Journal of the Atmospheric Sciences*, *59*(18), 2694–2712.
Wheeler, M., & Kiladis, G. (1999). Convectively-coupled equatorial waves: Analysis of clouds in the wavenumber-frequency domain. *Journal of the Atmospheric Sciences*, *56*, 374–399.